Icarus 320 (2019) 97–109

Contents lists available at ScienceDirect

Icarus

journal homepage: www.elsevier.com/locate/icarus

Photometry of Ceres and Occator faculae as inferred from VIR/Dawn data

A. Longobardo[a,*], E. Palomba[a,b], A. Galiano[a,c], M.C. De Sanctis[a], M. Ciarniello[a], A. Raponi[a], F. Tosi[a], S.E. Schröder[d], F.G. Carrozzo[a], E. Ammannito[e], F. Zambon[a], K. Stephan[d], M.T. Capria[a,b], E. Rognini[a], C.A. Raymond[f], C.T. Russell[g]

[a] INAF-IAPS, via Fosso del Cavaliere 100, Rome I-00133, Italy
[b] ASI-SSDC, via del Politecnico snc, Rome I-00133, Italy
[c] Università degli Studi di Roma Tor Vergata, Rome, Italy
[d] Institute for Planetary Research, Deutsches Zentrum fur Luft- und Raumfahrt (DLR), Berlin D-12489, Germany
[e] ASI-URS, via del Politecnico snc, Rome I-00133, Italy
[f] California Institute Technology JPL, Pasadena, CA 91109, USA
[g] UCLA, Los Angeles, CA 90095, USA

ARTICLE INFO

Article history:
Received 26 August 2017
Revised 12 February 2018
Accepted 15 February 2018
Available online 16 February 2018

Keywords:
Asteroid Ceres
Asteroids
Photometry
Spectroscopy

ABSTRACT

Spectral parameters of Ceres measured by the Dawn/VIR imaging spectrometer are studied as a function of illumination angles, by applying a semi-empirical method based on a statistical analysis of the VIR dataset acquired up to September 2016. The study also focuses on the photometry of the Occator faculae, i.e. the brightest spots of the Ceres surface, showing an albedo up to eight times the Ceres average. The considered semi-empirical approach takes into account the small extension (and hence small dataset) of this region and lays the groundwork to apply scattering models even on such a limited area.

The behavior of Ceres visible and infrared reflectance with phase angle is similar to other asteroids belonging to its same spectral class, i.e. C-type. The depth of the bands at 2.7 μm (phyllosilicates), 3.1 μm (ammonium), 3.4 μm (magnesium carbonates) and the infrared spectral slope linearly increase with phase angle, showing analogies with other asteroids and occurrence of phase reddening. The different behavior of the 3.9 μm band depth (also due to Mg carbonates), independent of illumination angles, could indicate that other carriers contribute to the 3.4 μm band and play a more important role in photometry outside the carbonate deposits.

The phase function of the Occator faculae is much steeper than expected from its high albedo. Mixture of bright and dark material and larger roughness can be at the basis of this result. The phyllosilicate bands show a steeper increase with phase angle with respect to the Ceres average, due to the lower presence of dark materials, and/or again larger roughness. The absence of trends with phase angles of the two carbonate bands and of the spectral slope suggests that carbonates do not produce phase reddening.

1. Introduction

The Dawn/NASA mission has been orbiting the (1) Ceres asteroid since 2015, after having performed a 1-year orbit around (4) Vesta (Russell and Raymond, 2011). The Dawn spacecraft hosts three instrument on boards, the Framing Camera (FC) (Sierks et al., 2011), the Visual and InfraRed mapping spectrometer (VIR) (De Sanctis et al., 2011) and the Gamma Ray and Neutron Detector (GRaND) (Prettyman et al., 2011), as well as the Radio Science Instrument, which all have allowed the investigation of the surface geology, topography and mineralogy as well as the elemental composition of the two asteroids.

The mission revealed that Ceres is a dark body, with an average reflectance at standard geometry (30° phase) of 0.03 at 0.55 μm (Ciarniello et al., 2017). Analyses on VIR data concluded that the average composition of Ceres is an unidentified dark component, magnesium-rich and ammoniated phyllosilicates and magnesium carbonates, partially confirming pre-Dawn results (e.g., Rivkin et al., 2011; Milliken and Rivkin, 2009). The absorption

* Corresponding author.
E-mail address: andrea.longobardo@iaps.inaf.it (A. Longobardo).

https://doi.org/10.1016/j.icarus.2018.02.022
0019-1035/

bands associated with these materials are centered at about 2.7 μm (the hydration band of phyllosilicates), 3.1 μm (due to ammonium), 3.4 μm and 4.0 μm, both due to carbonates (De Sanctis et al., 2015; 2016); dark materials are instead spectrally featureless. The bands at 2.7 μm and 3.1 μm show a moderate correlation, indicating that ammoniated phyllosilicates are diffusely distributed on the Ceres surface (Ammannito et al., 2016). However, other phases could be present on the Ceres surface and contribute to the 3.4 μm band (De Sanctis et al., 2016), even if their relative contribution to this band in different Ceres' locations has to be still assessed. However, other materials are observed in localized regions of the dwarf planet: for instance, the Ernutet crater (52°N, 45°E) shows occurrence of organics, as revealed by the deepening of the 3.4 μm band (De Sanctis et al., 2017a).

In terms of albedo, Ceres is a quite homogeneous body at global scale. However, many bright spots are found on its surface (Stein et al., 2018; Palomba et al., 2018). The composition of these regions could be different with respect to the Ceres average. This is mostly evident in the two brightest spots of Ceres, i.e. Cerealia and Vinalia Faculae, located inside the Occator crater (20°N 240°E). The spectra of these areas show a reflectance level up to eight times larger than the Ceres average (i.e. 0.24 at 0.55 μm), a deepening and a longward shift of the two carbonate bands (De Sanctis et al., 2016), as well as a longward shift of the 2.7 μm band (e.g., Longobardo et al., 2017a). This suggests that faculae consist of carbonate enrichments (with carbonate abundance larger than 50%), with occurrence of Na-carbonates in addition to (or instead of) Mg-carbonates (Carrozzo et al., 2018; Palomba et al., 2018) and of Al-phyllosilicates instead of Mg-phyllosilicates (as on the rest of Ceres surface). Their formation is ascribed to impact-induced heating and upwelling of volatile-rich materials and/or upwelling/excavation of heterogeneously distributed subsurface brines (Stein et al., 2018).

The interpretation of all these results has been supported by the application of a photometric correction on VIR spectra, i.e. the removal of illumination and viewing biases from the spectra. The correction has been based on the Hapke photometric model, and is described by Ciarniello et al. (2017). A similar model has been applied on Framing Camera data, as well (Schroeder et al. 2017), and on ground-based and Hubble Space Telescope data (Reddy et al., 2015; Li et al., 2006). The latter, however, were based only on observations at low phase angles (i.e., from 0° to 25°).

Photometric analysis on minor bodies has been performed also by applying approaches different than the Hapke modeling. For instance, the Minnaert (1941) modeling has been applied to Lutetia (e.g., Magrin et al., 2012; Li et al., 2013), and semi-empirical phase functions have been obtained for Vesta (e.g., Schroeder et al., 2013).

The aim of this work is to obtain a disk-resolved photometric behavior at moderate to high phase angle (i.e., from 20° to 60°) of the spectral parameters describing Ceres spectra, compare the results with those previously obtained on other asteroids explored by space missions, such as Gaspra (Helfenstein et al., 1994), Ida (Helfenstein et al., 1996), Mathilde (Clark et al., 1999), Eros (Li et al., 2004), Steins (Jorda et al., 2008), Annefrank (Hillier et al., 2011), Vesta and Lutetia (Longobardo et al., 2016), and photometrically characterize the Occator faculae. In particular, the latter goal allows highlighting and interpreting photometric differences between this peculiar region and the Ceres average.

The adopted approach is based on the statistical analysis of the instrument dataset, already developed for Vesta (Longobardo et al., 2014; 2015), Lutetia (Longobardo et al., 2016) and the Churyumov-Gerasimenko comet (Longobardo et al., 2017b). The Hapke's model could be not appropriate for analysis of small datasets covering only a few, discrete values of phase angles (such as the VIR data of Occator faculae), due to the large number of free parameters, which could be undetermined when retrieved over a small number of observations and hence deprived of their physical significance.[1] Nevertheless, the empirical photometric characterization obtained in this work permits to apply the Hapke's modeling by fixing some free parameters (Raponi et al., 2018). Moreover, our approach gives complementary results with respect to Hapke modeling even when applied on the entire Ceres surface, i.e.: 1) variations of photometric properties across the surface, which in turn may be ascribed to different physical and/or optical properties, and focus on particular regions; 2) direct comparison with disk-resolved phase functions of other asteroids, in order to infer the reasons for their differences (e.g., taxonomy, composition, grain size, roughness, albedo); 3) study of photometric behavior of spectral descriptors other than reflectance (e.g., band depth, spectral slope), which may add information about physical and optical properties of the surface. This approach is particularly important for the VIR dataset of Ceres, since it allows for obtaining a photometric function given by the product of a disk function and a polynomial curve, which, according to the photometric analysis on FC data, yields the highest quality global maps (Schroeder et al., 2017). Finally, this approach allows doing fast photometry, which could be applied for future missions, e.g. OSIRIS-REx (Lauretta et al., 2017).

The method is first applied to the entire Ceres surface, and then to the Occator faculae, in order to highlight and understand the nature of possible differences of the photometric properties between these peculiar regions and the rest of Ceres.

Data used for this study are presented in Section 2. Section 3 defines the spectral parameters studied, by applying the method described in Section 4. Sections 5 and 6 are devoted to results and their interpretations, respectively. Finally, in Section 7 conclusions are given.

2. Data

We used the data provided by the VIR mapping spectrometer, which is comprised of hyperspectral images, i.e. bi-dimensional spatial images acquired simultaneously at different wavelengths, and the corresponding observation geometries. The instrument is characterized by a single optical head, including a visible (0.25–1 μm, spectral sampling 1.8 nm) and an infrared (1–5 μm, spectral sampling 9.5 nm) channel.

All the spectra are calibrated in radiance factor *I/F*, by means of the procedure described by Filacchione and Ammannito (2014). In the following, we could also use the term "reflectance" in statements which apply to both reflectance and radiance factor. Procedures to remove spectral artifacts (Carrozzo et al., 2016) and the contribution of thermal emission (Raponi et al., 2018) are applied to VIR spectra.

The Dawn mission to Ceres is divided into different stages, characterized by a different spacecraft altitude and hence a different VIR spatial resolution. During the Approach (January to April 2015), these parameters were variable, then the spacecraft stabilized its altitude at ~13,000 km during the Rotational Characterization orbit (April–May 2015), corresponding to a spatial resolution of ~3400 m/pixel. A decreasing altitude and hence increasing spatial resolution were reached during the Survey (June 2015, altitude ~4400 km and resolution ~1100 m/pixel), High Altitude Mapping (HAMO, August to October 2015, altitude ~1470 km and resolution 360–400 m/pixel) and Low Altitude Mapping (LAMO, December 2015 to September 2016, altitude ~385 km and resolution 90–110 m/pixel) orbits.

[1] The Hapke's model has been applied by Schroeder et al. (2017) to study the photometry of Occator, but they considered the Framing Camera dataset, larger than the VIR one (35 versus 6 data points of Occator), and however they have found that a polynomial phase function reproduces the data better than the Hapke's model.

Since photometric functions can depend on the spatial resolution (e.g., Longobardo et al. 2014), we divided the entire dataset into a "low-resolution dataset" (including Approach, Rotational Characterization and Survey data) and a "high-resolution dataset" (including HAMO and LAMO data). However, when not specified, we refer to results obtained in the entire VIR dataset (without separation between low and high resolution data).

The VIR dataset includes about 5 million VIS spectra (about 3 million in low-resolution and 2 million in high-resolution), and about 22 million IR spectra (about 3 million in low-resolution and 19 million in high-resolution).

3. Tools

We studied the behavior with Solar incidence i, emission e and phase φ angles of the spectral parameters introduced in this section.

In order to monitor the photometric behavior in the entire VIR spectral range, we obtained phase functions of reflectance at six different wavelengths, three in the VIR visible domain, i.e. 0.55, 0.75 and 0.85 μm; and three in the VIR IR domain, i.e. 1.2, 1.9 and 2.3 μm. Longer wavelengths were not considered because of the presence of absorption bands in that spectral interval.

In particular, the study at 0.55 and 0.75 μm allows a comparison with phase functions of other asteroids, since most of them have been obtained at, or close to, these wavelengths (Longobardo et al., 2016). In order to maximize the signal-to-noise ratio, the radiance factor at each wavelength was calculated as the average on the four VIRTIS spectral pixels closer to that wavelength.

Then, the photometric behavior of band depths at 2.7, 3.1, 3.4 and 3.9 μm was studied. They were calculated as $1 - R_c/R_{con}$, being R_c and R_{con} the measured reflectance and the continuum at the band center (i.e., the band minimum after the continuum removal) wavelength (Clark and Roush, 1984).

The left shoulder of the 2.7 μm band was defined as the maximum reflectance between 2.63 and 2.70 μm, the right shoulder as the maximum reflectance of the 2nd degree polynomial fitting the spectrum between 2.80 and 3.00 μm, and the continuum as the straight line connecting the two shoulders.

The shape of the 3.1, 3.4 and 3.9 μm bands varies across the Ceres surface, especially on the bright spots and in particular on the Occator faculae, hence their definitions are challenging. The work by Galiano et al. (2017) was aimed at finding a definition of these bands, with the ability to reproduce them in dark, intermediate, bright and very bright (i.e. the Occator faculae) terrains of Ceres. In our work, we adopted their definitions for left and right shoulders, i.e.:

- For the 3.1 μm band, the reflectance maxima are calculated on 2nd order polynomials between 2.8 and 3.0 μm and 3.16 and 3.27 μm, respectively;
- For the 3.4 μm band, the reflectance maxima are between 3.05 and 3.36 μm and 3.55 and 3.68 μm, respectively;
- For the 3.9 μm band, the reflectance maxima are between 3.55 and 3.68 μm and 4.05 and 4.19 μm, respectively.

Continua are the straight lines connecting left and right shoulders (Fig. 1), whereas the band center is the minimum after the continuum removal, calculated between 3.0 and 3.16 μm (3.1 μm band), 3.36 and 3.55 μm (3.4 μm band), 3.68 and 4.05 μm (3.9 μm band), respectively.

In order to study the spectra phase reddening, we also studied the infrared spectral slope. This was defined according to the definition by Zambon et al. (2017), i.e. $(RADF_{1.9} - RADF_{1.2})/RADF_{1.9}(1.9 - 1.2)$, where $RADF_\lambda$ is the radiance factor at the wavelength λ.

The Occator faculae have been observed by VIR, especially during the HAMO stage. For most of this orbit, only the infrared channel operated. Therefore, for the Occator faculae case, we studied the photometric behavior of the infrared spectral parameters, only, and did not consider the visible spectral slope. The photometric behavior of the latter has already been studied by Ciarniello et al. (2017) for the Ceres average, and a comparison with Occator is, in fact, not possible.

4. Method

4.1. Ceres

4.1.1. Reflectance

The semi-empirical approach used to retrieve phase functions of Vesta (Longobardo et al. 2014) is based on a definition of reflectance families, which is in turn based on a statistical analysis of the instrument dataset. In detail, phase bins of 1 width are defined, each containing a number $N_{\Delta\varphi\ \mathrm{tot}}$ of values. Indicated with $N_{\Delta\varphi}$ the number of points with reflectance larger than a reference value R_φ, the percentile $P_{\Delta\varphi} = 100\ N_{\Delta\varphi}/N_{\Delta\varphi\mathrm{tot}}$ is a number comprised between 0 and 1 and is a function of R_φ and ranges between 0 and 1, i.e. $P_{\Delta\varphi}$ =xx% corresponds to the minimum reflectance R_φ of the xx% of the brightest pixels (if xx = 100, it corresponds to the minimum reflectance in the $\Delta\varphi$ bin). For each phase bins, nine values are considered (from 10 to 90, with a step of 10): each value represents a reflectance family. For each reflectance family, the corresponding phase function is retrieved.

This approach allows the retrieval of the phase functions of the brightest and darkest terrains of the studied surface. However, if the surface is homogeneous in terms of albedo or photometric properties, the phase functions corresponding to different reflectance families coincide within the errors. This is the case of the VIR dataset of Ceres, as already found for Lutetia (Longobardo et al. 2016) and Churyumov-Gerasimenko (Longobardo et al. 2017b), which is therefore photometrically homogeneous at large spatial scale. This is due to the fact that the total area occupied by all the Ceres bright spots is too small to be significant in a statistical analysis. Therefore, the study of photometry of the very bright faculae requires a separate study (see Section 4.2).

Given this, we did not adopt the definition of reflectance families, and instead calculated a single phase function describing the photometric behavior of each spectral parameter considered for the Ceres average.

In order to obtain the photometrically corrected reflectance, i.e. the reflectance at a defined observation geometry (e.g. $i = e = \varphi = 0°$), we used the common assumption (e.g., Schroeder et al., 2013) that I/F is the product of a disk function $D(i, e, \varphi)$, modelling the topography contribution, and a phase function $F(\varphi)$, describing the behavior with phase angle.

The correction is hence applied in two steps:

1. Selection of the disk function that best removes the topography influence (i.e. i and e) from the reflectance, among those defined in literature, i.e. Lambert, Lommel-Seeliger, Akimov (e.g. Schroeder et al., 2013; Shkuratov et al., 2011), and retrieval of the equigonal albedo I/FD, henceforth R/D. The best disk function minimizes the slope of the residual trends R/D vs. i and R/D vs. e. In particular, we consider that no residual trend with incidence and emission arises if the absolute value of this slope (calculated by means of linear fits) is lower than $1{\cdot}10^{-4}$ (i.e., a reflectance variation lower than 0.01, which is our resolution of photometric parameters, defined in next sub-section).
2. Retrieval of the phase function, by fitting the median values of R/D, calculated on phase angle bins of 1° width (whereas their

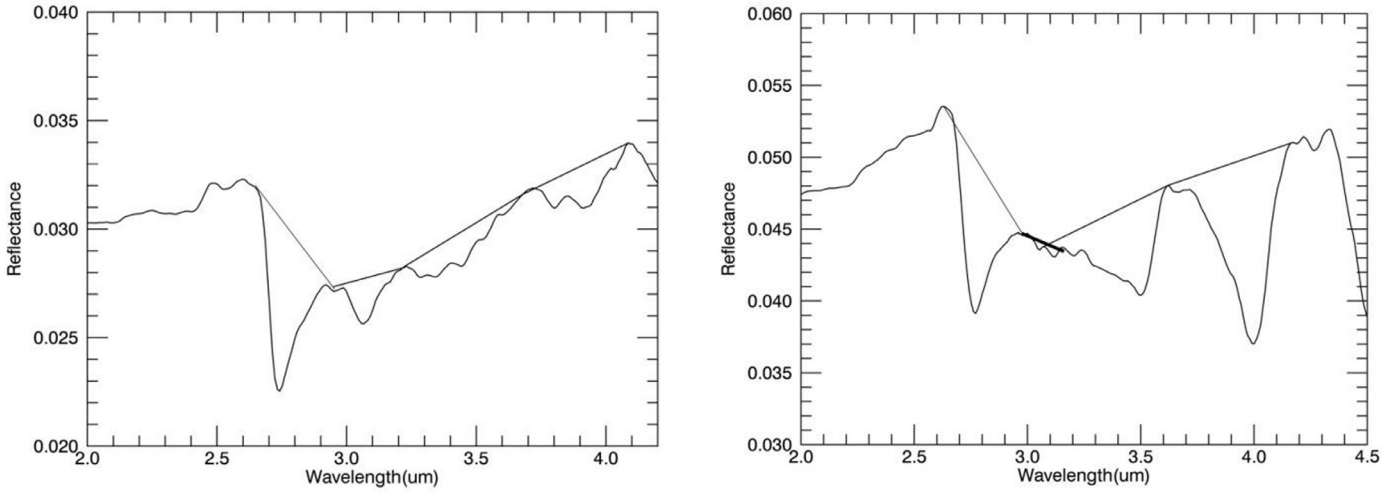

Fig. 1. Definition of continua of the absorption bands in Ceres' VIR spectrum, in the case of a typical Cerean terrain (left) and of an Occator facula spectrum (right). In the right spectrum, the continuum of the 3.1 μm band is thicker.

uncertainty is calculated as standard deviation of the mean), as a function of phase angle, by means of a 3rd degree polynomial, i.e.:

$$R/D = A_0 + b\varphi + c\varphi^2 + d\varphi^3 \quad (1)$$

The equigonal albedo at phase angle 0° was obtained as $A_0 = R/D - b\varphi - c\varphi^2 - d\varphi^3$and mapped on the Ceres surface. Note that this quantity does not coincide with the geometric albedo, because the minimum phase angle in our dataset is 12.3°, hence the opposition effect is not modeled (i.e., the behavior between 0° and 12.3° is assumed to follow the Eq. (1)).

This process was applied at all the wavelengths considered in this study.

4.1.2. Photometric parameters

The comparison of disk-resolved phase functions of Ceres with other asteroids has been performed by adopting two photometric parameters describing these functions, as defined by Longobardo et al. (2016): the *I/F* at 0.75 μm retrieved at 30° phase (*R30*) and the steepness of the phase function between 20° and 60° phase angles, henceforth Phase Curve Slope (*PCS*), defined as *1-R60/R20*, where *R60* and *R20* are the *I/F* at 60° and 20° phase angle, respectively. These parameters have been already calculated by Longobardo et al. (2016) for all the other asteroids explored by space missions, except Itokawa (observed only at phase angles lower than 40°). In the *R*30 vs. *PCS* scatterplot, asteroids belonging to the same spectral class are grouped together, and the general trend observed is a *PCS* decreasing for increasing *R30*, due to the increasing role of multiple scattering (Longobardo et al., 2016).

In order to obtain these parameters on Ceres, we recalculated the Ceres phase function at 0.75 μm, by modeling *I/F* as a function of φ, instead of *R/D*, in order to obtain a reliable comparison with the available phase functions, which model the behavior of the radiance factor. However, the influence of incidence and emission angles on the retrieval of photometric parameters is generally minor (Longobardo et al., 2016; 2017b). The uncertainties on *R*20, *R*30 and *R*60 are given by the difference between modeled and calculated values, and the uncertainty on *PCS* is obtained by propagating the errors on *R*20 and *R*60.

The *R30* and *PCS* parameters were used also to evaluate the influence of spatial resolution on the retrieval of Ceres phase functions. They were calculated on the phase functions obtained from the analysis on the entire, low-resolution and high-resolution datasets, respectively. However, since the visible high-resolution dataset does not include phase angles larger than 40°, it is not possible to calculate *R60* and hence *PCS* in this case. Therefore, the evaluation of the role of spatial resolution was made at 1.2 μm, once verified that the photometric behavior at this wavelength is very similar to visible wavelengths (Section 5.1).

4.1.3. Band depths and spectral slope

The photometric behavior of band depths and spectral slope was studied by applying the same process described in Section 4.1.1, skipping Step 1. According to our assumptions, disk function is a multiplying factor and, in principle, does not affect these parameters that are basically given by reflectance ratios. The validity of this assumption was verified a posteriori, when we observed no trends in phase-corrected band depths (or phase-corrected spectral slopes) with incidence and emission angles.

4.2. Occator faculae

To apply the same method described in Section 4.1.1 to the Occator faculae regions, we had to overcome two issues.

The first one is the selection of spectra of Cerealia and Vinalia faculae. The faculae are in fact recognizable from their larger albedo, but the albedo is indeed the quantity we want to retrieve. Since the faculae are characterized by occurrence of sodium carbonates, showing a longward shift of the 3.9 μm band center, we selected all the spectra included in the Occator crater region (defined by latitude boundaries 18.2°N and 20.7°N and longitude boundaries 237°E and 242°E), whose band center of the carbonate bands is located at 4 μm or longward.

The second issue is the low number of selected observations (about 5000), with some phase bins showing only few observations to be reliable for a statistical analysis. Therefore, in order to retrieve the faculae phase function, we considered only phase bins with at least 50 spectra. Due to the lack of bins corresponding to phase angles larger than 60°, a linear fit is sufficient to model the faculae phase function. We extracted *R30* and *PCS* from this fit.

After the reflectance correction, the A_0 values are available. We used these values to select the spectra of the faculae in order to study the photometric behavior of the other spectral parameters. In particular, we selected all the spectra showing A_0 at 1.2 μm larger than 0.13. This threshold excludes all the spectra with short band centers (i.e. < 3.98 μm), and most of spectra with band centers between 3.98 and 4.00 μm (Fig. 2). Moreover, we verified a posteriori

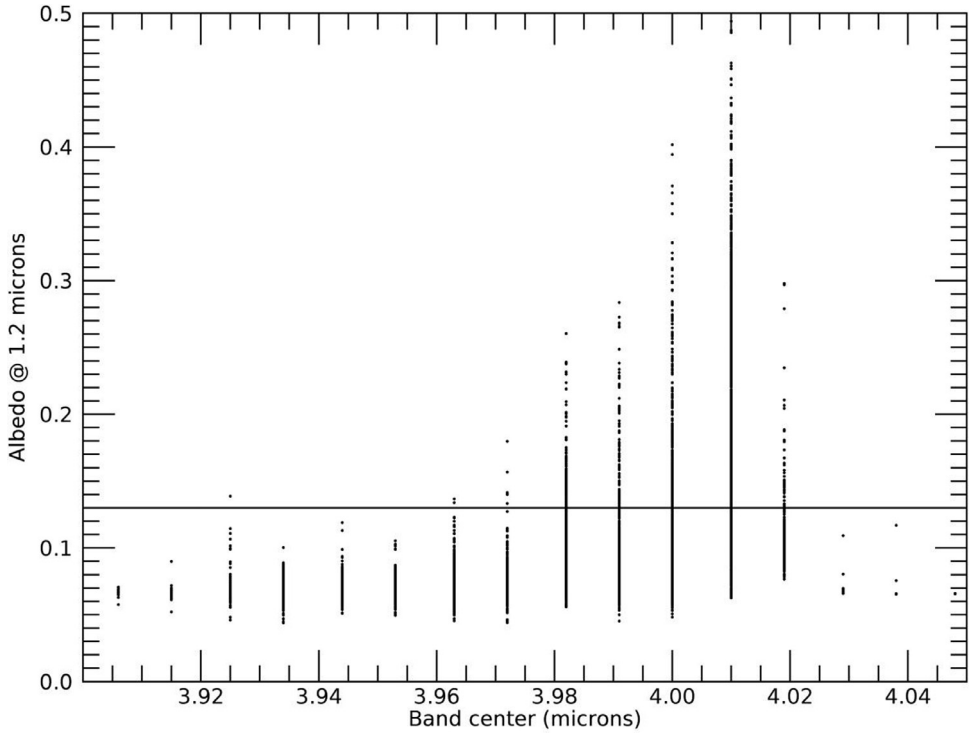

Fig. 2. Albedo at 1.2 μm as a function of the 3.9 μm band center for all the observations included in the Occator crater region (latitude between 18.2°N and 20.7°N and longitude between 237°E and 242°E). The discrete values of band center reflect the VIR spectral sampling. A_0 values larger than 0.13 (horizontal straight lines) exclude short band centers.

Table 1
Slope of the reflectance behavior with incidence and emission angles before (i.e. *I/F* column) and after (i.e. *R/D* columns) the application of different disk functions. The residual slope is better than the acceptability threshold (i.e. $1{\cdot}10^{-4}$) in both Lommel-Seeliger (LS) and Akimov cases.

Trend	*I/F*	*R/D* (Lambert)	*R/D* (LS)	*R/D* (Akimov)
R/D vs. *i*	$-2.5{\cdot}10^{-4}$	$1.2{\cdot}10^{-4}$	$-9.9{\cdot}10^{-5}$	$-3.4{\cdot}10^{-5}$
R/D vs. *e*	$4.4{\cdot}10^{-4}$	$2.9{\cdot}10^{-4}$	$-5.8{\cdot}10^{-5}$	$1.8{\cdot}10^{-5}$

Table 2
Parameters of the Ceres phase functions at different wavelengths.

Wavelength (μm)	b ($0{\cdot}10^{-3}$)	c ($0{\cdot}10^{-5}$)	d ($0{\cdot}10^{-8}$)	R^2
0.55	-1.69 ± 0.04	1.90 ± 0.10	-8.2 ± 0.7	1.00
0.75	-1.69 ± 0.05	1.88 ± 0.09	-8.1 ± 0.7	1.00
0.85	-1.62 ± 0.05	1.76 ± 0.10	-7.4 ± 0.7	1.00
1.20	-1.52 ± 0.03	1.70 ± 0.08	-7.6 ± 0.5	1.00
1.90	-1.51 ± 0.04	1.65 ± 0.08	-7.2 ± 0.5	1.00
2.30	-1.55 ± 0.03	1.68 ± 0.08	-7.2 ± 0.5	1.00

that the reflectance phase function obtained for these observations is similar within errors, with the phase function obtained by applying the band center selection (see Fig. 7 in Section 5.2).

5. Results

5.1. Ceres

5.1.1. Reflectance

Table 1 shows the slopes of the linear fits *R/D* vs. *i* and *R/D* vs. *e*, before and after the application of the Lambert, Lommel-Seeliger (LS) and Akimov disk functions. In order to minimize the phase angle influence, we calculated these trends in a narrow phase angle interval, i.e. between 30° and 50°. The values indicating the substantial absence of residual trends (i.e., lower than $1{\cdot}10^{-4}$, in absolute value) are highlighted. For simplicity, we considered only non-parametric disk functions. Since some of them are already able to remove trends with incidence and emission angle, there was no need to consider parametric and more complicated disk functions.

Whereas the application of the Lambert disk function overcorrects the reflectance, introducing a positive trend with incidence angle, LS and Akimov disk functions allow for obtaining equigonal albedo values which could be considered independent of incidence and emission. In particular, the slopes obtained for the Akimov-corrected equigonal albedo are lower, therefore we applied this disk function for all the wavelengths considered, i.e.:

$$D(\beta,\gamma,\varphi)=\cos\frac{\varphi}{2}\cos\left[\frac{\pi}{\pi-\varphi}\left(\gamma-\frac{\varphi}{2}\right)\right]\frac{(\cos\beta)^{\varphi/\pi-\varphi}}{\cos\gamma}, \quad (2)$$

where $\gamma=arctan\frac{\cos i-\cos e\cos\varphi}{\cos e\sin\varphi}$ is the photometric longitude, $\beta=arccos\frac{\cos e}{\cos\gamma}$ is the photometric latitude and φ is the phase angle (Shkuratov et al., 1999). D is an unitless quantity which is equal to 1 for a normal observation ($i=e=\varphi=0°$, in this case $I/F=R/D$) and decreases at increasing illumination and observation angles.

The parameters of Eq. (1) are shown in Table 2 for the different wavelengths analyzed, together with the R^2 parameter, indicating the goodness of fit. As the latter is 1, the polynomial curve very well fits the data at all the wavelengths.

The obtained Ceres phase function (at 1.2 μm) is shown in Fig. 3, whereas the reflectance distribution across the surface before (i.e. *I/F*) and after (i.e. A_0) the photometric correction is shown in Fig. 4. The correction is able to remove the reflectance discontinuities between images taken under different phase angles. In the A_0 map, we observed that the Ceres is overall uniform in terms of reflectance, and the brightest and the darkest large-scale terrain are the Vendimia Planitia, located at equatorial latitudes and at longitudes between 90° and 160°, and the region eastward of Vendimia Planitia, located at longitudes between 170° and 220°. The Occator faculae region is enclosed in the black square in

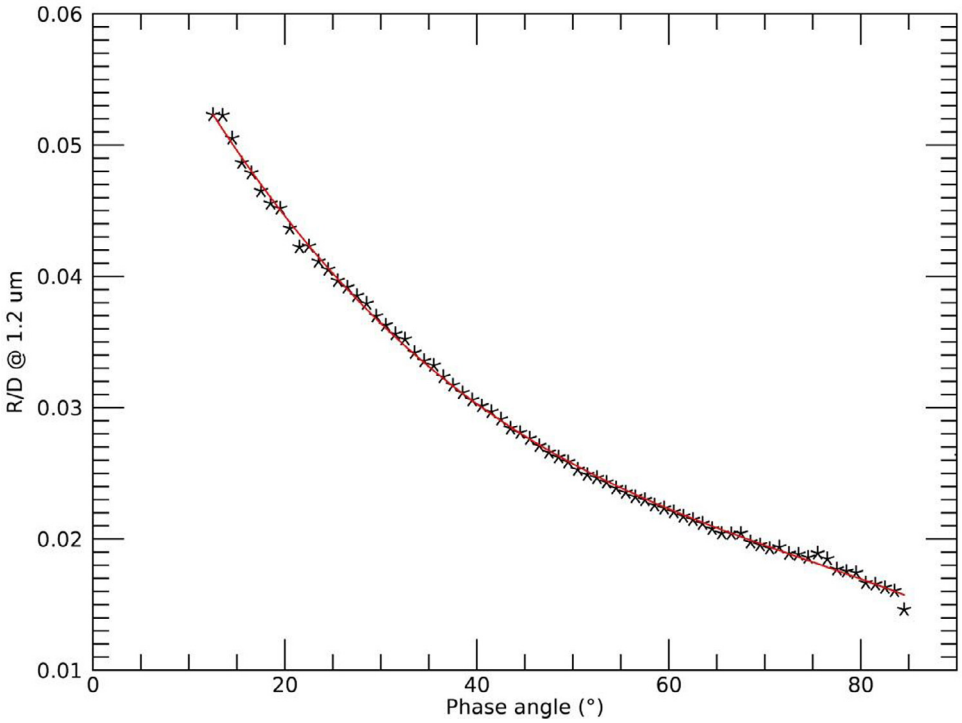

Fig. 3. Equigonal albedo as a function of phase angle (asterisks) and modeled phase function (curve). Error bars are included within the points' size.

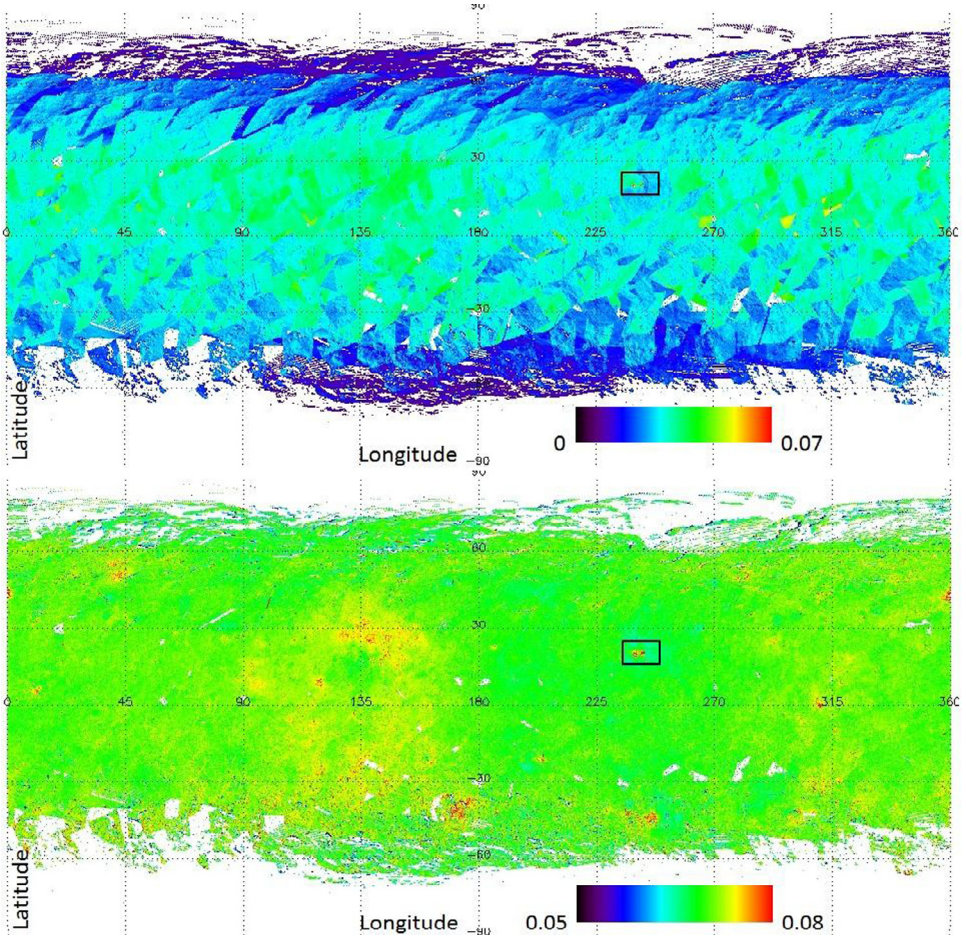

Fig. 4. Distribution of *I*/*F* (top, before correction) and A_0 (bottom, after correction) at 1.2 μm. The black square includes the Occator faculae region. The mosaics are composed of 712 images, acquired in different mission stages. The color (green/blue) discontinuities observed in the top figure are due to overlapping of images taken under different phase angles. These discontinuities are removed from the photometric correction (bottom figure). (For interpretation of the references to color in this figure legend, the reader is referred to the web version of this article.)

Table 3
Photometric parameters of asteroids visited by space missions. Taxonomy refers to the classification by De Meo et al. (2009). Uncertainty on *R30* is always lower than 0.01. Photometric parameters of Ceres are the same at 0.55 and 0.75 μm. For each wavelength, photometric parameters were calculated on the entire, low-resolution (LR) and high-resolution (HR) dataset.

Asteroid	Taxonomy	Wavelength (μm)	R30	PCS	Phase function reference
Vesta (dark terrain)	V	0.75	0.15	68 ± 6	Longobardo et al. (2016)
Vesta (average)	V	0.75	0.18	58 ± 2	Longobardo et al. (2016)
Vesta (bright terrain)	V	0.75	0.22	48 ± 1	Longobardo et al. (2016)
Steins	Xe	0.63	0.19	50 ± 6	Jorda et al. (2008)
Ida	S	0.56	0.06	67 ± 5	Helfenstein et al. (1996)
Annefrank	S	0.63	0.10	56 ± 4	Hillier et al. (2011)
Eros	S	0.55	0.08	59 ± 5	Li et al. (2004)
Gaspra	S	0.56	0.08	58 ± 5	Helfenstein et al. (1994)
Lutetia	Xk	0.75	0.07	50 ± 2	Longobardo et al. (2016)
Mathilde	C	0.70	0.02	77 ± 7	Clark et al. (1999)
Ceres (entire dataset)	C	0.55–0.75	0.03	71 ± 7	This work
Ceres (LR dataset)	C	0.55–0.75	0.03	68 ± 7	This work
Ceres (HR dataset)	C	0.55–0.75	0.03	N/A	This work
Ceres (entire dataset)	C	1.2	0.03	64 ± 7	This work
Ceres (LR dataset)	C	1.2	0.03	69 ± 7	This work
Ceres (HR dataset)	C	1.2	0.03	62 ± 7	This work
Occator	C	1.2	0.12	64 ± 8	This work

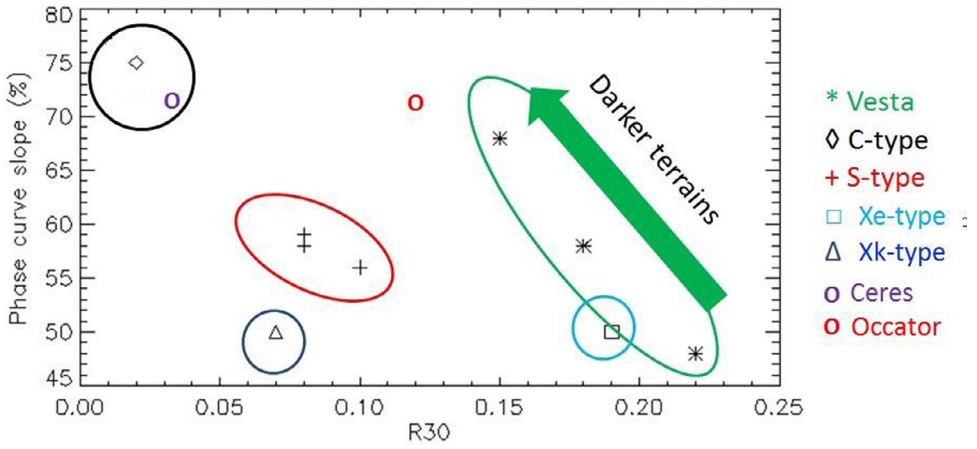

Fig. 5. PCS as a function of *R30* at 0.75 μm for different asteroids and for the Occator region. Errors are not shown for clarity. Ida is not shown because its photometric parameters could be biased since obtained from observations at much better spatial resolution with respect to the other asteroids. Occator's photometric parameters are extrapolated, by assuming that the variation between visible and infrared spectral range is the same as the rest of Ceres.

Fig. 4 and is by far the brightest region of Ceres (its reflectance is out of color scale).

The albedo distribution is in very good agreement with that found by Ciarniello et al. (2017), by applying the Hapke method, as well as with distribution derived from Framing Camera (Schroeder et al., 2017) and HST (Li et al., 2006) observations.

Moreover, the phase functions retrieved at the six wavelengths (i.e., *b, c* and *d* parameters in Table 2) led to corrected reflectance values within errors (see Section 5.1.2), hence we can assume a unique phase function for the entire spectral range analyzed.

5.1.2. Photometric parameters

The photometric parameters calculated for Ceres and for the other asteroids are shown in Table 3 and Fig. 5. Details about the retrieval of *R30* and *PCS* for other asteroids are found in Longobardo et al. (2016).

The photometric parameters of Ceres were calculated in the VIR visible domain, in particular at 0.55 and 0.75 μm, in order to compare them with other asteroids. The retrieved values of *R30* and *PCS* are the same at the two wavelengths. Moreover, they were calculated at 1.2 μm, to enable a comparison with the Occator region, mainly observed by the VIR IR channel.

An increasing spatial resolution can change the *PCS* value. For example, Ida was observed at better spatial resolution (i.e. down to 25 m) and was characterized by a larger *PCS* (Longobardo et al., 2016). In order to evaluate the role of spatial resolution also on the Ceres phase function, the retrieval of photometric parameters was performed on the entire, low-resolution and high-resolution VIR datasets. However, visible high-resolution data cover phase angles not larger than 40°; therefore *R60*, and hence *PCS*, cannot be obtained.

Ceres is located in the *R30-PCS* scatterplot close to the C-type Mathilde. The variation of photometric parameters with spatial resolution is well within errors. This is not an obvious result, because photometric similarity between Ceres and other C-type asteroids observed so far has been based on low phase angle observations, only (i.e., lower than 20°, Shevchenko and Belskaya, 2010). In addition, this scatterplot led to different results for objects expected to be grouped together, such as the comets, characterized by similar albedo but very different photometric behavior, due to different roughness and surface evolution (Longobardo et al., 2017b).

5.1.3. Band depths and spectral slope

Since we obtained that phase functions do not depend on spatial resolution, we can assume that the same occurs for photometric behavior of other spectral parameters, too. Therefore, the analysis of these parameters was performed on the entire VIR dataset, without separation in high-resolution and low-resolution dataset.

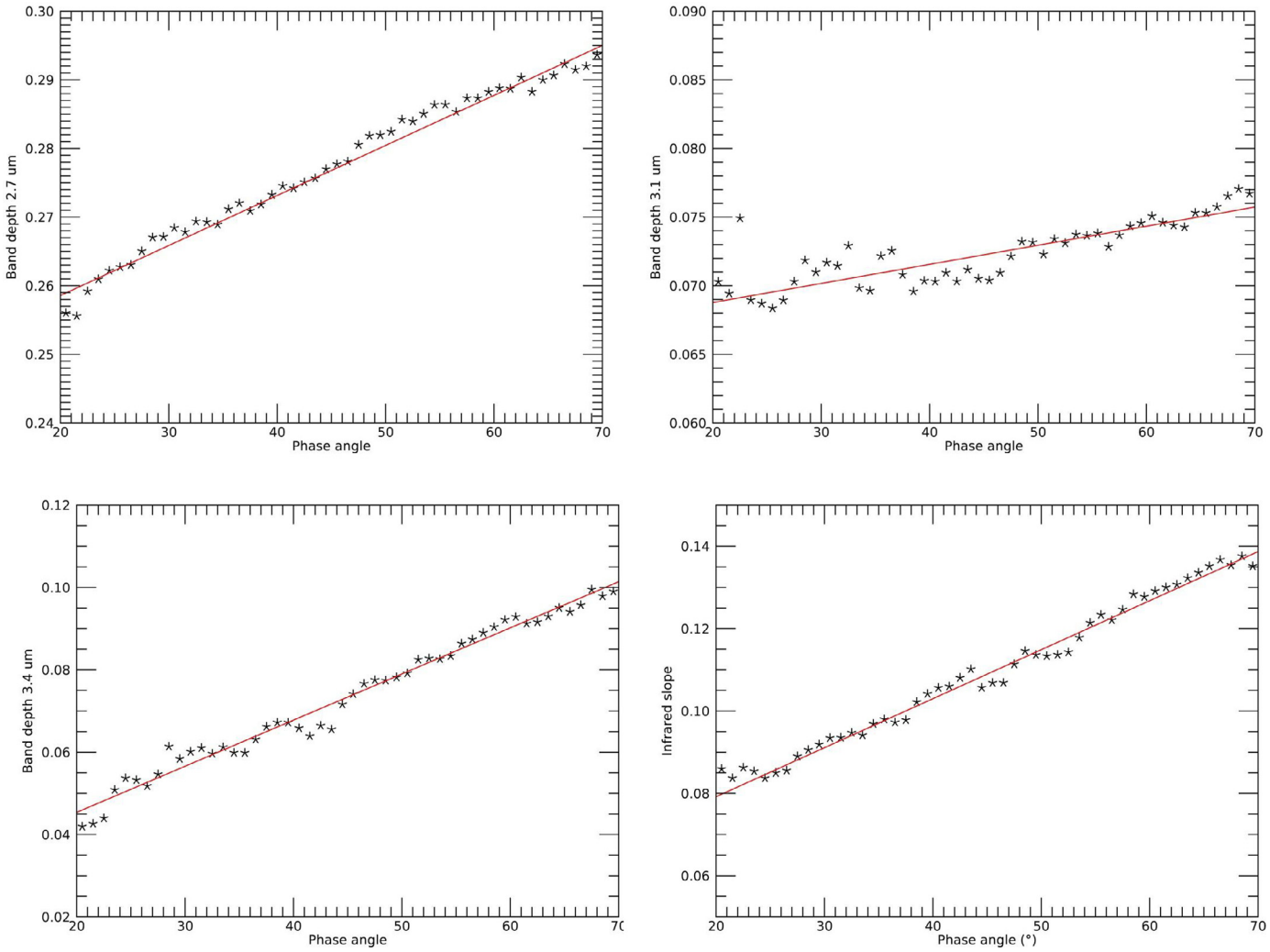

Fig. 6. From top to bottom: behavior with phase angle of band depths at 2.7 μm, 3.1 μ, 3.4 μm and of infrared slope, for the Ceres average, and related linear fits (solid lines). Error bars are included within the points' size.

Table 4
Increasing rate S with phase of the different spectral parameters considered in this work, calculated for the Ceres average and the Occator faculae. "No trend" means R^2 close to zero, i.e. lower than 0.15.

Spectral parameter	Ceres average		Occator faculae	
	S	R^2	S	R^2
2.7 μm band depth	$(7.29 \pm 0.15) \cdot 10^{-4}$	0.98	$(1.7 \pm 0.9)\ 0 \cdot 10^{-3}$	0.50
3.1 μm band depth	$(1.39 \pm 0.11)\ 0 \cdot 10^{-4}$	0.70	No band	
3.4 μm band depth	$(1.09 \pm 0.03)\ 0 \cdot 10^{-3}$	0.98	No trend	
3.9 μm band depth	No trend	No trend		
Infrared slope	$(1.19 \pm 0.03)\ 0 \cdot 10^{-5}$	0.98	No trend	

Almost all of the considered parameters linearly increase with the phase angle (Fig. 6), as the 3.9 μm band depth is the only parameter not showing this trend.

We calculated the relation between each spectral parameter P and the phase angle, by means of a linear fit $P = P_0 + S\varphi$.

Fits were calculated in the phase angle interval 20°–70°, including the most populated phase angle bins. The best linear fits are also shown in Fig. 6.

The S values corresponding to each parameter and the R^2 of the linear fit are shown in Table 4.

The high R^2 values indicated that the linear fit reproduces very well the observed data. Only for the 3.1 μm band depth, the fit is slightly worse, probably due to the very small increase with phase.

5.2. Occator faculae

Due to the small dataset considered for this analysis, and hence due to the small number of phase bins useful for it, a linear fit is the most indicated to reproduce the Occator faculae phase function (Fig. 7): in fact, the uncertainty on fitted parameters is in this case not larger 10–15%, whereas it becomes of 100% or larger when polynomial fits are applied. However, since the fit is calculated on a few points, the R^2 is 0.50.

The corresponding photometric parameters are shown in Table 3. Whereas *R30* is four times the Ceres average, the *PCS* is essentially the same.

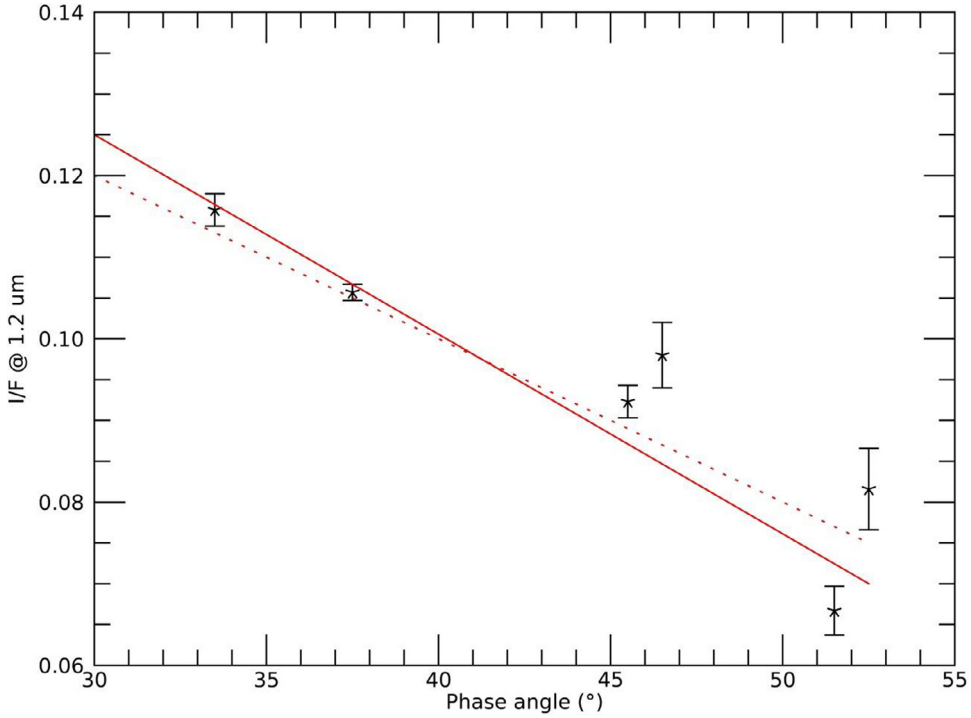

Fig. 7. Phase function of the *I/F* at 1.2 μm for the Occator faculae region. The dotted line is the phase function obtained by selecting the Occator's pixels basing on albedo instead of 3.9 μm band center.

In order to compare the faculae's photometric parameters with those obtained for the other asteroids in the visible range, we assume the Occator faculae's *PCS* at 0.75 μm equal at the Ceres average's *PCS* at the same wavelength. This value is plotted in Fig. 5. Our assumption is corroborated by the following observational evidences:

- Ceres average and Occator faculae have the same *PCS* at 1.2 μm, despite their different *R30*;
- *PCS* is mainly related to *R30* (anti-correlation), and this value is almost constant among both Ceres and Occator spectra. Nevertheless, in the case of Occator a slight bluing is observed between 0.75 and 1.2 μm (De Sanctis et al., 2016), therefore the Occator faculae's *PCS* might be larger.

However, the value plotted in Fig. 5 is already much larger than other asteroids having a similar *R30*, i.e. the S-type asteroids. Thus this region deviates from the classical behavior of the steepness of phase function, which generally decreases at increasing albedo, as inferred from both ground (Shevchenko and Belskaya, 2010) and space (Longobardo et al., 2016) observations, and does not have a photometric equivalent among the asteroids.

The similar steepness of phase function between Occator and the rest of Ceres confirms the results obtained by the photometric analysis from Framing Camera data (Schroeder et al., 2017).

Concerning the other spectral parameters, the band depth at 2.7 μm is the only one that preserves an increasing trend with phase angle. The increasing rate *S* is two times that found for the Ceres average (Fig. 8), even if the uncertainty is larger (due to the lower number of observations). The 3.1 μm band is not observed in this region (De Sanctis et al., 2016; Longobardo et al., 2017a), because this band is ascribed to ammoniated phyllosilicates, whereas in Occator ammonium is present in a different form (Raponi et al., 2018). The other two band depths have a very similar behavior, independent of phase angle (Fig. 9). The infrared slope does not show variations with phase angle, neither.

6. Discussion

6.1. Ceres

For each wavelength, we could consider a single phase function modeling the photometric behavior of Ceres. In other words, Ceres is photometrically uniform, and variations of optical and physical properties among the surface are, when present, limited to a few, small regions. This result indicates that events capable to heavily change these properties are very old and/or were very localized.

The reflectance is very well modeled by the product of the Akimov disk function and the 3rd degree polynomial (Eq. (1)), with a R^2 parameter of 1. This result is in agreement with the photometric analysis on FC data of Ceres, which concluded that the combination of the Akimov disk function and a polynomial allows for obtaining the best quality maps (Schroeder et al. 2017).

The agreement within errors of the phase functions retrieved at different wavelengths is justified by the small reflectance variation across the visible and NIR spectrum, i.e., lower than 10% (De Sanctis et al., 2015). It is thus likely that the optical properties of the surface do not change in this spectral range.

No variation (or variation within the errors) of the phase function between low- and high- spatial resolution is also observed. For comparison, in the case of the VIR dataset of Vesta, the "high-resolution (HR)" *PCS* exceeds the *PCS* calculated on the entire dataset of five times the error (Longobardo et al., 2016). Analogously, the higher *PCS* of Ida with respect to the other asteroids has been ascribed to the highest spatial resolution of its observations (Longobardo et al., 2016). This would occur because of the more important role of local topography, which would cause shadowing, especially at larger phase angles. The reasons for the different behavior observed for Ceres could be one or more of the following:

- The spatial resolution of the Ceres HR images is not small enough to appreciate variations due to local topography. The best spatial resolution achieved for Ceres is 100 m, whereas

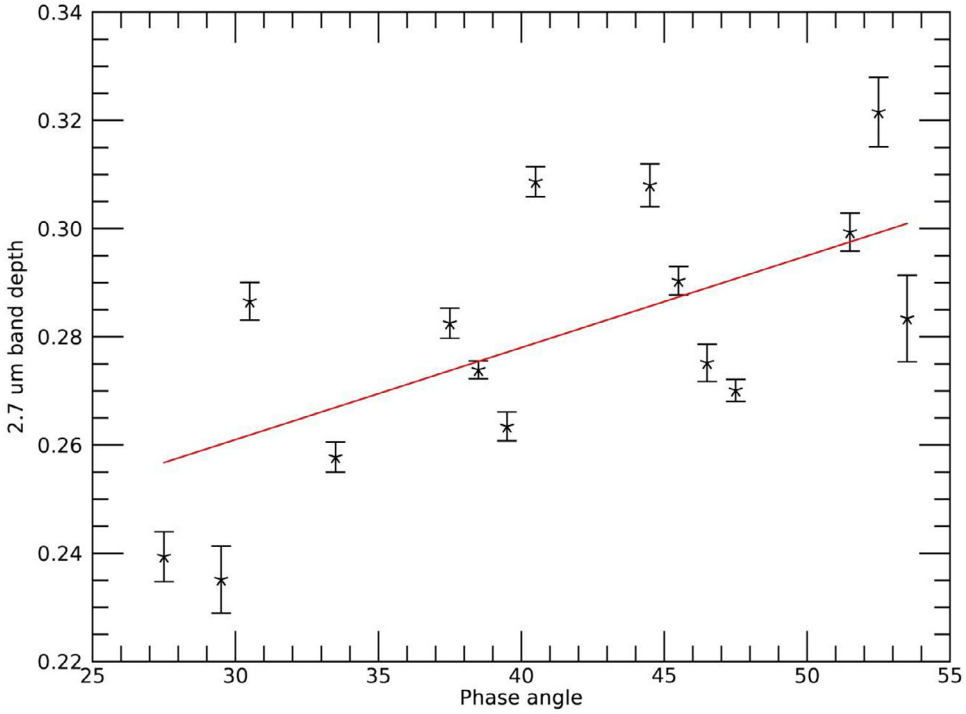

Fig. 8. Behavior with phase angle of band depth at 2.7 μm for the Occator faculae region, and related linear fit (solid line).

it is 50 m for Vesta (Russell et al., 2012) and 25 m for Ida (Helfenstein et al., 1996). Moreover, the spatial resolution ratio, e.g., between Survey and HAMO observations of Ceres is about 10, whereas for Vesta it is about 15 (Russell and Raymond, 2011). Therefore, the difference between the HR and LR datasets is highlighted in the case of Vesta.

- Physical properties (e.g., roughness) of the surface are similar at small and large scales. This would be in agreement with the low roughness of Ceres features observed even in LAMO FC images (Schroeder et al., 2017).
- Whereas the multiple reflections occurring at a small scale of a bright surface could render the radiation extinct, on a dark body such as Ceres the role of multiple scattering is negligible (e.g., Ciarniello et al. 2017).

The asteroid closest to Ceres in the *R30* vs. *PCS* scatterplot (Fig. 5) is Mathilde, belonging to the same taxonomic class, i.e. C-type, according to results by Ciarniello et al. (2017). This scatterplot is once again demonstrated to be useful in discriminating different asteroid taxonomies. In particular, Ceres is slightly brighter than Mathilde, and its phase function is slightly flatter, according to the general anti-correlation between *R30* and *PCS* observed for the minor bodies. Since comparison with ground-observations suggests that Mathilde is a good representative of the C-type spectral class (Shevchenko and Belskaya, 2010), we may consider Ceres to be a bright C-type asteroid. This would mean that the slight photometric difference between Ceres and Mathilde would lie in their different optical properties, instead of physical properties (such as grain size and roughness), which may be similar among the C-type asteroids.

The linear increase of band depths with phase angle has already been observed for other asteroids, e.g., Vesta (Longobardo et al., 2014; Schroeder et al, 2014), and could be due to: (a) steeper phase function of the reflectance corresponding to band center, due to the larger absorption involved; (b) phase reddening (different reddening of the two band shoulders). Therefore, the lack of this increasing trend for the 3.9 μm, due to carbonates, could be justified by one or more of the following reasons: a) abundance of carbonates is too small to produce a band depth behavior with phase which is suppressed by the presence of opaques (according to De Sanctis et al., 2015, carbonate and opaque abundances are on average lower than 20% and larger than 70%, respectively); b) the difference between phase functions at the shoulder and band center wavelengths is minimal, due to brightness of carbonates; c) carbonates do not contribute to phase reddening. We discard hypothesis a) because independence of phase angle is observed even in the Occator faculae, where carbonate is the most abundant component (see next sub-section). However, in both the remaining cases, we should observe an independence of phase angle also for the 3.4 μm, as well ascribed to carbonates. The different photometric behavior of this band hence suggests that other phases contribute to this spectral feature, as suggested by its complex shape (De Sanctis et al., 2015). In addition, it gives us the possibility of understanding the relative contribution of carbonates on this band, giving clues on the Ceres surface composition. We could not however discard that the procedure of thermal removal masks the photometric behavior of the 3.4 μm band.

Finally, the phase behavior of the infrared slope indicates the occurrence of phase reddening, as already demonstrated in previous works (Ciarniello et al., 2017). In particular, the increment S is in very good agreement with that obtained by Ciarniello et al. (2017), by applying the Hapke method (in that case $S = 1.5 \cdot 10^{-5}$, and the slight difference is justified by the fact that they calculated the slope between 1.2 and 2.0 μm, instead of 1.2 and 1.9 μm).

6.2. Occator faculae

Different from what was expected from its large albedo, the steepness of the phase function of the Occator faculae is the same as the rest of Ceres. This means that Eq. (1) can be used to obtain photometrically-corrected reflectance even for those regions much brighter than the Ceres average. A similar result was found from the photometric analysis on FC data (Schroeder et al., 2017). This

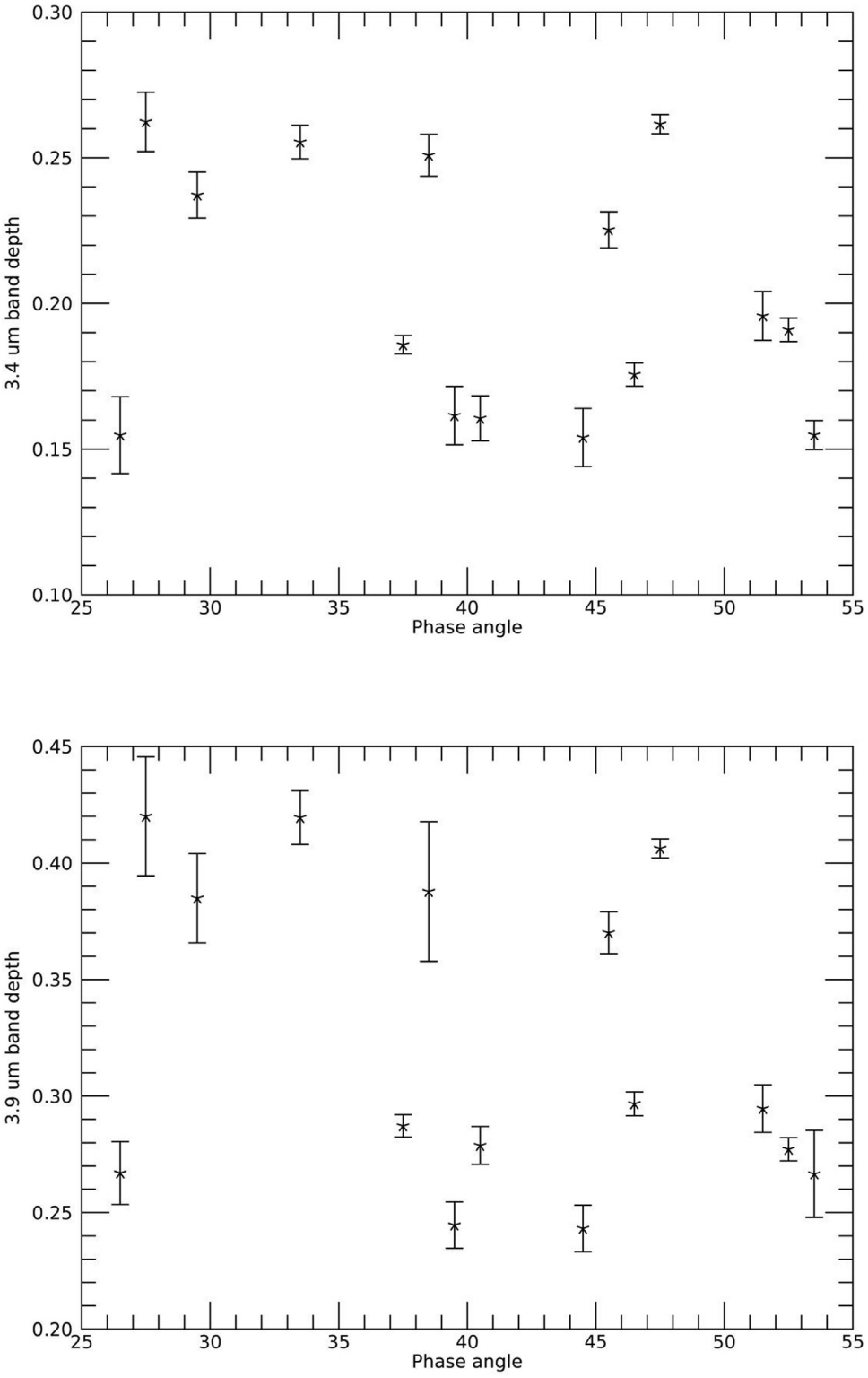

Fig. 9. Band depth at 3.4 μm (top) and at 3.9 μm (bottom) as a function of phase angle for the Occator faculae region.

result could not be obtained by applying the Hapke's model on VIR data of Occator, because the small number of observation geometries would led to largely undetermined Hapke's free parameters. On the other hand, the obtained result allowed to make assumptions in applying the Hapke's linear mixing model and infer some physical properties of Occator, as done by Raponi et al. (2018).

The *R30* vs. *PCS* scatterplot (Fig. 5) shows the lack of an asteroid spectral class equivalent to the Occator faculae. Nevertheless, photometric parameters of the dark terrains of Vesta are not much different from the *R30* and *PCS* values obtained for the faculae. Both Vesta dark terrains and Ceres bright spots are composed of a mixture of dark and bright materials. In both cases, the abundance of the dark component, i.e., carbonaceous chondrites for

Table 5
Summary of photometric behavior of the spectral parameters analyzed in this work and related interpretations.

Spectral parameter	Ceres average	Occator faculae	Interpretations
VIS/NIR reflectance	Compatible with C-type asteroids	Same slope of phase curve wrt Ceres, despite of the larger albedo	Larger roughness on faculae; mixture of dark and bright materials
2.7 μm band depth	Increasing with phase	Steeper increasing with phase wrt Ceres (2 times larger)	Larger roughness; lower abundance of opaques on faculae
3.1 μm band depth	Increasing with phase	No observed band	Commonly observed behavior of band depths
3.4 μm band depth	Increasing with phase	No behavior	Another carrier could contribute to the 3.4 μm band on Ceres average
3.9 μm band depth	No behavior	No behavior	Carbonates do not produce phase reddening; carbonate brightness
IR slope	Phase reddening	No phase reddening	Carbonates do not produce phase reddening

Vesta (McCord et al., 2012) and unidentified for Ceres, is 20–30% (Palomba et al., 2014; De Sanctis et al., 2016; Raponi et al., 2018). The bright component of Vesta is represented by HED achondrites, whose abundance in dark terrains is 70–80% (Palomba et al., 2014). The abundance of carbonates (bright components) on the faculae is a bit lower (i.e., 50–70%), due to occurrence of other materials, i.e. phyllosilicates, ammonium (De Sanctis et al., 2016; Raponi et al., 2018). We could infer that the location in the *R30* vs. *PCS* scatterplot, characterized by moderate to high values of both parameters, does not correspond to specific asteroid taxonomies, but to mixtures of them.

However, the high steepness of the faculae's phase function could also be due to different physical properties. A larger grain size and/or roughness can in fact increase the *PCS*.

We applied the method by Raponi et al. (2018), based also on the outcomes of this paper, to estimate the average grain size of the selected faculae region, finding a value of 60 ± 40 μm. The same method led to an average grain size of the Ceres surface of about 100 μm. Hence the anomalous *PCS* of the Occator faculae cannot be ascribed to grain size.

Due to the occurrence of many fractures inside the faculae (Buczkowski et al., 2017; Stein et al., 2018), the faculae's roughness is instead larger, as might be confirmed by the large value of the Hapke's roughness parameters obtained from analysis of FC data (Schroeder et al., 2017). Therefore, roughness can be identified as a possible reason of the observed photometric behavior.

The steeper increase of the band depth at 2.7 μm could be ascribed to the much lower abundance of dark materials, i.e., 20–30% in the faculae versus 60–80% in the rest of Ceres (De Sanctis et al., 2015). In fact, the presence of opaques suppresses not only the band, but also its behavior with phase. It is possible that the phyllosilicates band depth shows the photometric behavior observed on the Occator faculae, and this increasing trend is weakened elsewhere due to a larger amount of dark components. Larger roughness could also justify the steeper increase of band depth with phase angle. Coarser grains may be another possible reason, but it is discarded from the results shown above.

The 3.4 and 3.9 μm band depths are independent of phase angle. Since natrite (sodium carbonate) is the most abundant component in the faculae (De Sanctis et al., 2016; Palomba et al. 2018), carbonate is the main carrier of the 3.4 μm band, which in fact shows the same photometric behavior of the 3.9 μm band, i.e. no trend with phase angle (Fig. 9). This is different from the photometric behavior of the 3.4 μm band depth on the Ceres average, and again points toward an additional component (at least) contributing to this band and having a major role in the photometric behavior of this band outside the carbonate deposits.

The independence of the carbonate bands of phase could be due to the high brightness and/or to the lack of phase reddening for these materials. The latter is confirmed by the lack of an increasing trend of the infrared slope with phase, indicating that no phase reddening occurs in the Occator faculae region.

7. Conclusions

Except a few localized regions, Ceres is photometrically homogeneous, and this could be related to old age or small extensions of events modeling the Ceres surface.

The photometric function given by the product of the Akimov disk function and a polynomial phase function well reproduces the VIR observation of Ceres, as already observed for the Framing Camera data. No spectral variations of the phase function are observed between 0.55 and 2.3 μm, indicating that the surface optical properties are constant in this spectral range. Furthermore, the phase function is independent of spatial resolution, differently to other, brighter asteroids (e.g., Vesta and Ida). This could be due either to the low albedo or to the small-scale smoothness of the surface. Future disk-resolved observations of dark asteroids, such as Bennu (Lauretta et al., 2017) and Ryugu (Ishiguro et al., 2014), could confirm one or more of these hypotheses.

The shape of the Ceres phase function is in agreement with the C-type taxonomy, in particular that Ceres could be a "bright" C-type asteroid. This is a new result, because the photometric similarity between Ceres and other C-type asteroids has been based so far only on low phase angle observations, whereas we found that this agreement occurs even for phase angle up to 60°. The obtained result suggests Ceres and other C-type asteroids show similar physical properties or, however, that physical properties play a minor role in photometry of C-type asteroids.

The strength of the bands at 2.7, 3.1 and 3.4 μm and the infrared spectral slope (1.2–1.9 μm) linearly increase with phase angle, indicating the presence of phase reddening and a photometric behavior similar to other asteroids. The different behavior of the band depth at 3.9 μm could indicate that on the spectrum of the Ceres average, other materials (in addition to carbonates) contribute to the 3.4 μm band. As a matter of fact, when carbonates are the dominant component (i.e., in the Occator faculae), the two bands show the same photometric behavior. Therefore, photometry of the 3.4 μm band allows giving a preliminary assessment the relative contribution of carbonates to this band without need of radiative transfer model.

The lack of the linear increase with phase observed in the Occator faculae for the two carbonate band depth and the infrared spectral slope would indicate that sodium carbonates do not produce phase reddening. An analysis on laboratory spectra could be required to confirm this result. An alternative explanation is that carbonates are too bright, and the larger multiple scattering masks their phase behavior.

Moreover, Occator faculae are photometrically very peculiar because the steepness of their phase function is much higher than expected from their large albedo. A similar photometric behavior is observed on the dark terrains on Vesta (Longobardo et al., 2014), that, similarly to Cerealia and Vinalia faculae, are composed of a mixture of bright and dark material. The large steepness could be also caused by larger roughness. Roughness could also produce the

steeper increase of the band depth at 2.7 μm (due to phyllosilicates) with phase observed in the Occator faculae. This behavior could, however, be due also to the low abundance of dark materials, which generally suppresses the phase variation of band depths.

Table 5 summarized the photometric behaviors of the spectral parameters considered in this work, observed for the Ceres average and the Occator faculae, and their possible interpretations.

Acknowledgments

VIR is funded by the Italian Space Agency-ASI and was developed under the leadership of INAF-Istituto di Astrofisica e Planetologia Spaziali, Rome-Italy. The instrument was built by Selex-Galileo, Florence-Italy. The authors acknowledge the support of the Dawn Science, Instrument, and Operations Teams.

Sharon Uy (UCLA, USA) is thanked for the manuscript revision.

References

Ammannito, E., 2016. Distribution of phyllosilicates on the surface of Ceres. Science 353, 6303. doi:10.1126/science.aaf4279.

Buczkowski, D.H., et al., 2017. The geology of the Occator quadrangle of dwarf planet Ceres: floor-fractured craters and other geomorphic evidence of cryomagmatism. Icarus in press. doi:10.1016/j.icarus.2017.05.025.

Carrozzo, F.G., et al., 2016. Artifacts reduction in VIR/Dawn data. Rev. Sci. Instrum. 87, 12. doi:10.1063/1.4972256.

Carrozzo, F.G., 2018. Nature, formation and distribution of carbonates on Ceres. Sci. Adv. in press.

Ciarniello, M., et al., 2017. Spectrophotometric properties of dwarf planet Ceres from VIR onboard Dawn mission. Astron. Astrophys. 598, A130.

Clark, R.N., Roush, T.L., 1984. Reflectance spectroscopy – Quantitative analysistechniques for remote sensing applications. J. Geophys. Res. 89, 6329–6340.

Clark, B.E., et al., 1999. NEAR photometry of Asteroid 253 Mathilde. Icarus 140, 53–65.

De Meo, F.E., et al., 2009. An extension of the Bus asteroid taxonomy into the near-infrared. Icarus 202 (1), 160–180.

De Sanctis, M.C., et al., 2011. The VIR Spectrometer. Space Sci. Rev. 163, 329–369.

De Sanctis, M.C., et al., 2015. Ammoniated phyllosilicates with a likely outer system origin on (1) Ceres. Nature 528, 241–244.

De Sanctis, M.C., et al., 2016. Bright carbonate deposits as evidence of aqueous alteration on (1) Ceres. Nature 536, 54–57.

De Sanctis, M.C., et al., 2017a. Localized aliphatic organic material on the surface of Ceres. Science 355 (6326), 719–722.

Filacchione, G., Ammannito, E., 2014. Dawn VIR calibration document Version 2.4 https://sbn.psi.edu/archive/dawn/vir/DWNVVIR_I1B/DOCUMENT/VIR_CALIBRATION/VIR_CALIBRATION_V2_4.PDF.

Galiano, A., et al., 2017. Continuum definition for 3.05, 3.4 and 4.0μm absorption bands in Ceres spectra. Adv. Space Res. in press. doi:10.1016/j.asr.2017.10.039.

Helfenstein, P., et al., 1994. Galileo photometry of Asteroid 951 Gaspra. Icarus 107, 37–60.

Helfenstein, P., et al., 1996. Galileo photometry of Asteroid 243 Ida. Icarus 120 (1), 48–65.

Hillier, J.K., et al., 2011. Photometric modeling of Asteroid 5535 Annefrank from Stardust observations. Icarus 211 (1), 546–552.

Ishiguro, M., et al., 2014. Optical Properties of (162173) 1999 JU3: In Preparation for the JAXA Hayabusa 2 Sample Return Mission. Astrophys. J. 792 (1), 74.

Jorda, L., et al., 2008. Asteroid 2867 Steins. I. Photometric properties from OSIRIS/Rosetta and ground-based visible observations. Astron. Astrophys. 487 (3), 1171–1178.

Lauretta, D., et al., 2017. OSIRIS-REx: sample return from asteroid (101955) Bennu. Space Sci. Rev. 212 (1–2), 925–984.

Li, J., et al., 2004. Photometric analysis of Eros from NEAR data. Icarus 172, 415–431.

Li, J.-Y., et al., 2006. Photometric analysis of 1 Ceres and surface mapping from HST observations. Icarus 182 (1), 143–160.

Li, J-Y., et al., 2013. Global photometric properties of Asteroid (4) Vesta observed with Dawn Framing Camera. Icarus 226 (2), 1252–1274.

Longobardo, A., et al., 2014. Photometric behavior of spectral parameters in Vesta dark and bright regions as inferred by the Dawn VIR spectrometer. Icarus 240, 20–35.

Longobardo, A., et al., 2015. Mineralogical and spectral analysis of Vesta's Gegania and Lucaria quadrangles and comparative analysis of their key features. Icarus 259, 72–90.

Longobardo, A., et al., 2016. Disk-resolved photometry of Vesta and Lutetia and comparison with other asteroids. Icarus 267, 204–216.

Longobardo, et al., 2017a. Mineralogy of the Occator quadrangle. Icarus, in press. doi:10.1016/j.icarus.2017.09.022.

Longobardo, et al., 2017b. Photometric behaviour of 67P/Churyumov-Gerasimenko and analysis of its pre-perihelion diurnal variations. Mon. Not. R. Astron. Soc., in press. doi:10.1093/mnras/stx1803.

Magrin, S., et al., 2012. (21) Lutetia spectrophotometry from Rosetta-OSIRIS images and comparison to ground-based observations. Planet. Space Sci. 66 (1), 43–53.

McCord, T.B., et al., 2012. Dar kmaterial on Vesta from the infall of carbonaceous volatile-rich material. Nature 491 (7422), 83–86.

Milliken, R.E., Rivkin, A.S., 2009. Brucite and carbonate assemblages from altered olivine-rich materials on Ceres. Nat. Geosci. 2, 258–261.

Minnaert, M., 1941. The reciprocity principle in lunar photometry. Astrophys. J. 93 (May), 403–410.

Palomba, E., et al., 2014. Composition and mineralogy of dark material units on Vesta. Icarus 240, 58–72.

Palomba, et al., 2018. Compositional differences among Bright Spots on the Ceres surface. Icarus in press. doi:10.1016/j.icarus.2017.09.020.

Prettyman, T.H., et al., 2011. Dawn's gamma ray and neutron detector. Space Sci. Rev. 163, 371–459.

Raponi, A., et al., 2018. Mineralogy of Occator crater on Ceres and insight into its evolution from the properties of carbonates, phyllosilicates, and chlorides. Icarus in press. doi:10.1016/j.icarus.2018.02.001.

Reddy, V., et al., 2015. Photometric properties of Ceres from telescopic observations using Dawn Framing Camera color filters. Icarus 260, 332–345.

Rivkin, A.S., et al., 2011. The surface composition of Ceres. Space Sci. Rev. 163 (1–4), 95–116.

Russell, C.T., Raymond, C.A., 2011. The Dawn mission to Vesta and Ceres. Space Sci. Rev. 163 (1-4), 3–23.

Russell, C.T., et al., 2012. Dawn at Vesta: testing the protoplanetary paradigm. Science 336 (6082), 684–686.

Schroder, S.E., et al., 2013. Resolved photometry of Vesta reveals physical properties of crater regolith. Planet. Space Sci. 85, 198–213.

Schroeder, S.E., et al., 2014. In-flight calibration of the Dawn Framing Camera II: flat fields and stray light correction. Icarus 234, 99–108.

Schroeder, S.E., et al., 2017. Resolved spectrophotometric properties of the Ceres surface from Dawn Framing Camera images. Icarus 288, 210–225.

Shevchenko, V.G., Belskaya, I.N., 2010. Regolith of low albedo asteroids from photometric data. Regolith on Solar System bodies Workshop December 1–3 2010.

Shkuratov, Y.G., et al., 1999. Opposition effect from Clementine data and mechanisms of backscatter. Icarus 141, 132–155.

Shkuratov, Y., et al., 2011. Optical measurements of the Moon as a tool to study its surface. Planet. Space Sci. 59, 1326–1371.

Sierks, H., et al., 2011. The Dawn Framing Camera. Space Sci. Rev. 163, 263–327.

Stein, N., et al., 2018. Characteristic, Formation and Evolution of Faculae (Bright Spots) on Ceres. Icarus doi:10.1016/j.icarus.2017.10.014.

Zambon, F., et al., 2017. Mineralogical analysis of Quadrangle Ac-H-10 Rongo on the Dwarf Planet Ceres. in press doi:10.1016/j.icarus.2017.09.021.